Supporting Information

Hydrogel-confined Fe-MOF nanozyme sensor chip for matrix-tolerant colourimetric screening of malathion in Chinese medicinal matrices

Zhiyi Zhou[1#], Xiaoye Liu[1#], Jia Yang[1], Mingyi Xue[1], Xinru Liu[1], Rong Rong[1,2*], Tiantian Si[1,2,*]

[1]*Shandong University of Traditional Chinese Medicine, Jinan, 250355, China*

[2]*Key Laboratory of Traditional Chinese Medicine Classical Theory, Ministry of Education, Shandong Key Laboratory of Digital Traditional Chinese Medicine，Shandong University of Traditional Chinese Medicine*

S1. Construction of the Fe-MOF/sodium alginate (SA) hydrogel sensor chip

Specifically, 1.35 g of $FeCl_3 \cdot 6H_2O$ and 0.33 g of terephthalic acid (H_2BDC) were dissolved in 30 mL of N,N-dimethylformamide (DMF) and stirred vigorously for 30 min at room temperature. The homogeneous solution was transferred to a 50 mL Teflon-lined autoclave and heated at 110 °C for 24 h to yield an Fe-MOF precipitate. After cooling, the product was centrifuged and washed three times each with DMF and

Zhiyi Zhou[1#]and Xiaoye Liu[1#] contributed equally to this work.

*Corresponding author. *E-mail address*: rosierong@163.com (R. Rong); 60030153@sdutcm.edu.cn; 13051471988@163.com (T. Si)

ethanol at 8000 rpm for 10 min to remove unreacted ligands and byproducts. The resulting dark brown powder was dried under vacuum at 60 °C for 12 h and ground to obtain the orange–red Fe-MOF nanozyme powder. Considering the possible structural variability of Fe–BDC frameworks synthesised from $FeCl_3$ and terephthalic acid under solvothermal conditions, the obtained material is conservatively referred to as an Fe-MOF nanozyme throughout this work.[39]

The process began with the preparation of a homogeneous suspension: sodium alginate (SA) powder was dissolved in deionized water under magnetic stirring to obtain a 2% (w/v) stock solution. Subsequently, the synthesized Fe-MOF nanozyme powder was incorporated into the SA solution and subjected to ultrasonication for 10 min, achieving a uniform dispersion with a final nanozyme concentration of 10 mg mL^{-1}. For chip assembly, a clean plastic substrate (PET, 2 cm × 2 cm) served as the support. A 15 μL aliquot of the Fe-MOF/SA mixture was precisely dispensed onto the substrate center, followed by the immediate addition of 50 μL of 2% (w/v) $CaCl_2$ solution to initiate ionic crosslinking. The chip remained undisturbed for 90 s to allow complete gelation, after which any residual $CaCl_2$ solution was carefully removed using filter paper. This yielded a stable, round, and semitransparent hydrogel spot approximately 3 mm in diameter firmly anchored to the chip surface.

S2. Detailed Characterization Conditions

The morphology of the blank hydrogel and the Fe-MOF-loaded hydrogel was characterized by scanning electron microscopy (SEM) using a ZEISS Sigma 360 microscope (Carl Zeiss, Germany). Cross-sectional images were collected in secondary electron mode, and the samples were cut to expose the cross-section prior to direct analysis without additional Au/C sputter coating. The specific surface area and pore structure were evaluated by BET analysis on a Micromeritics ASAP 2460 surface area

and porosity analyzer (Micromeritics, USA) using N_2 at 77 K; before measurement, the powder samples were degassed at 120 °C for 10 h, and the full-pore analysis mode was used to obtain the surface area and pore-size distribution. Powder X-ray diffraction (XRD) patterns were recorded on a Bruker D8 Advance diffractometer (Bruker, Germany) equipped with a Cu target over the 2θ range of 5–90° at a scanning rate of 2° min^{-1}, and the powdered samples were lightly ground before analysis for phase identification and crystallinity evaluation. X-ray photoelectron spectroscopy (XPS) measurements were performed on a Thermo Scientific K-Alpha spectrometer (Thermo Fisher Scientific, USA) in the routine survey-plus-high-resolution mode; high-resolution spectra were collected for O, Fe, and C to analyze the surface elemental composition and chemical states of the samples, and valence-band spectra were additionally acquired when required. Fourier-transform infrared (FTIR) spectra were recorded on a Thermo Fisher Scientific Nicolet iS20 spectrometer (Thermo Fisher Scientific, USA) over the wavenumber range of 400–4000 cm^{-1}, and the spectra were exported in absorbance mode for subsequent analysis and comparison.

S3. Smartphone image acquisition and CIE LAB colour analysis

All colourimetric images were acquired using the same smartphone throughout the study to minimise device-dependent variation. The hydrogel sensor chip was placed on a clean white background and photographed under a fixed white LED illumination source. The smartphone camera was positioned vertically above the sensing area at a constant distance of 15 cm. During image acquisition, the focus, exposure, shooting distance, illumination geometry, and white-balance settings were kept unchanged for all measurements. Images were collected after the prescribed colour-development time and were saved under the same image format and resolution settings. For colour analysis, the acquired images were imported into ImageJ software (version 1.8.0). A circular region of interest (ROI) was selected within the central area of the hydrogel

sensing spot, avoiding the edge of the hydrogel and any visible reflection or shadow. The same ROI size and selection criteria were applied to all images. The RGB values extracted from the ROI were converted to the CIE LAB colour space, and the b* coordinate was used as the analytical readout because it provided a sensitive and reproducible description of the blue-to-yellow colour variation associated with the H_2O_2–TMB chromogenic reaction. For each measurement, the reported b* value was obtained from replicate chips or replicate images as specified in the corresponding experiment. To reduce imaging-related bias, all chips compared within the same experiment were photographed under identical conditions in the same imaging session whenever possible. Blank, standard, and matrix-spiked samples were processed using the same imaging and ROI-selection procedure. No manual adjustment of brightness, contrast, saturation, or colour balance was performed before quantitative analysis.

S4. HPLC conditions for malathion quantification and chromatographic cross-validation

Malathion was quantified by high-performance liquid chromatography (HPLC) both in the post-adsorption supernatants and in the pretreated spiked extracts used for chromatographic cross-validation of the proposed method. The analysis was performed on a C18 reversed-phase column (250 × 4.6 mm, 5 μm). The mobile phase consisted of methanol and water (70:30, v/v) under isocratic elution at a flow rate of 1.0 $mL \cdot min^{-1}$. The detection wavelength was set at 220 nm, the column temperature was maintained at 30 °C, and the injection volume was 10 μL. Quantification was carried out using an external calibration curve established under the same chromatographic conditions. Each concentration level was analysed in triplicate.

S5. Detailed Adsorption Experiments

To investigate malathion adsorption, both kinetic and equilibrium adsorption

experiments were carried out. A 1 $mg \cdot mL^{-1}$ malathion stock solution was prepared by dissolving 10.0 mg of malathion in 10 mL of methanol. This stock was further diluted with the same buffer to prepare malathion solutions at 0.30 and 0.40 $mg \cdot mL^{-1}$ for the kinetic study, and at 0.01, 0.05, 0.08, 0.10, 0.20, 0.30, and 0.40 $mg \cdot mL^{-1}$ for the equilibrium isotherm study.

For the kinetic adsorption experiments, 10.00 mL of each malathion solution (0.30 or 0.40 $mg \cdot mL^{-1}$) was transferred into a 15 mL centrifuge tube, and exactly 5.00 mg of Fe-MOF nanozyme was added to each tube. The mixtures were vortexed for 1 min to ensure uniform dispersion and then placed in a thermostatic shaker at 25 °C and 180 rpm. At predetermined time intervals (5, 10, 15, 20, 25, and 30 min), samples were collected and immediately centrifuged at 10000 rpm for 10 min to separate the nanozyme. The clear supernatants were analysed by high-performance liquid chromatography (HPLC) to determine the residual malathion concentration, and the adsorption capacity at time t (q_t) was calculated accordingly.

For the equilibrium adsorption experiments, 10.00 mL of each malathion solution (0.01, 0.05, 0.08, 0.10, 0.20, 0.30, or 0.40 $mg \cdot mL^{-1}$) was treated in the same manner by adding 5.00 mg of Fe-MOF nanozyme. After vortex mixing, the tubes were shaken at 25 °C and 180 rpm for 2 h, which had been confirmed in preliminary experiments to be sufficient for reaching adsorption equilibrium. After adsorption, the suspensions were centrifuged at 10000 rpm for 10 min, and the clear supernatants were analysed by HPLC. The equilibrium adsorption capacity (q_e) was calculated according to Eq. (1).

To further elucidate the adsorption behaviour of malathion on Fe-MOF, the kinetic data were fitted using the pseudo-first-order (2) and pseudo-second-order (3) models, whereas the equilibrium data were fitted using the Langmuir (4) and Freundlich (5) isotherm models. The corresponding equations are listed below:

$$q_e = \frac{(C_0 - C_e)v}{m} (1)$$

$$ln(q_e - q_t) = ln\, q_e - k_1 t (2)$$

$$\frac{t}{q_t} = \frac{1}{k_2 q_e^2} + \frac{t}{q_e} (3)$$

$$\frac{C_e}{q_e} = \frac{1}{K_L q_{max}} + \frac{C_e}{q_{max}} (4)$$

$$ln\, q_e = ln\, K_F + \frac{1}{n} ln(C_e) (5)$$

Where q_e (mg·g^{-1}) is the equilibrium adsorption capacity; q_t (mg·g^{-1}) is the adsorption capacity at time t; C_0 (mg·mL^{-1}) is the initial concentration of malathion; C_e (mg·mL^{-1}) is the equilibrium concentration of malathion in solution; V (mL) is the volume of the adsorption solution; m (g) is the mass of Fe-MOF; t (min) is the adsorption time; k_1 (min^{-1}) is the rate constant of the pseudo-first-order model; k_2 (g·mg^{-1}·min^{-1}) is the rate constant of the pseudo-second-order model; q_{max} (mg·g^{-1}) is the maximum monolayer adsorption capacity; K_L (mL·mg^{-1}) is the Langmuir adsorption constant related to adsorption affinity; K_F is the Freundlich constant indicative of adsorption capacity; and n is the Freundlich intensity factor reflecting surface heterogeneity.

S6. Calibration Curve Construction and Limit of Detection

The calibration curve was constructed by plotting the CIE LAB b* value against lgc, where C is the malathion concentration in ng mL^{-1}. Linear regression gave b* = 13.03 lgC − 29.96 with R^2 = 0.993. Because lgC was used as the independent variable, the LOD was calculated as the concentration corresponding to b*blank + 3σ, where σ is the standard deviation of ten blank measurements.

S7. Detailed Real Sample Pretreatment

Chrysanthemum, honeysuckle, and coptis samples were pulverized and passed through a 40-mesh sieve. A 5.0 g portion of each powdered sample was extracted with 25 mL methanol by shaking at room temperature for 30 min, followed by centrifugation at 8000 rpm for 10 min. The resulting supernatant was subjected to a C18 cartridge-assisted clean-up/pass-through step to reduce gross matrix interference while retaining a pretreated herbal-extract background. Before sample loading, the C18 cartridge was sequentially conditioned with 5 mL methanol and 5 mL water. The methanolic extract was then passed through the conditioned cartridge, and the cleaned flow-through fraction was collected directly, rather than using a retention–elution procedure. The collected fraction was filtered through a 0.22 μm membrane and used for hydrogel-chip detection and HPLC cross-validation. This procedure was intended to remove part of the co-extracted hydrophobic pigments and particulate matrix components, but not to eliminate the herbal matrix completely; therefore, the subsequent standard-addition and matrix-effect experiments were performed in a pretreated authentic matrix background.

Spike-recovery, matrix-effect, and precision experiments were conducted using the pretreated herbal extracts. Each concentration level was analysed in eleven replicates (n = 11), and the results are reported as mean ± standard deviation (SD). The spike recovery, matrix effect (ME), and relative standard deviation (RSD) were calculated as follows:

$$\text{Recovery (\%)} = (C_{found} / C_{spiked}) \times 100\% \qquad (6)$$

$$\text{ME (\%)} = ((S_{matrix} / S_{solvent}) - 1) \times 100\% \qquad (7)$$

$$\text{RSD (\%)} = (SD / Mean) \times 100\% \qquad (8)$$

where C_{found} is the measured concentration in the spiked sample; C_{spiked} is the nominal spiked concentration; Smatrix and Ssolvent are the slopes of the matrix-

matched and solvent-based calibration curves, respectively; SD is the standard deviation of replicate measurements; and Mean is the arithmetic mean of the replicate results. Negative ME values indicate signal suppression, whereas positive values indicate signal enhancement. In this manuscript, $|ME| \leq 20\%$ was considered negligible.

S8. Calculations for Fig. 4 and Fig. 5

All calculations were based on the CIE LAB b* readout. Response deviation for Fig. 4D:

$$\text{Deviation (\%)} = |b^*\text{matrix} - b^*\text{solvent}| / |b^*\text{solvent}| \times 100 \quad (9)$$

where b*matrix is the response in a herbal extract, and b*solvent is the solvent response at the same malathion concentration.

Relative signal intensity for Fig. 5B:

$$\text{RSI (\%)} = |b^*\text{malathion+interferent}| / |b^*\text{malathion only}| \times 100 \quad (10)$$

RSI values within 85–115% were considered acceptable for front-end screening.

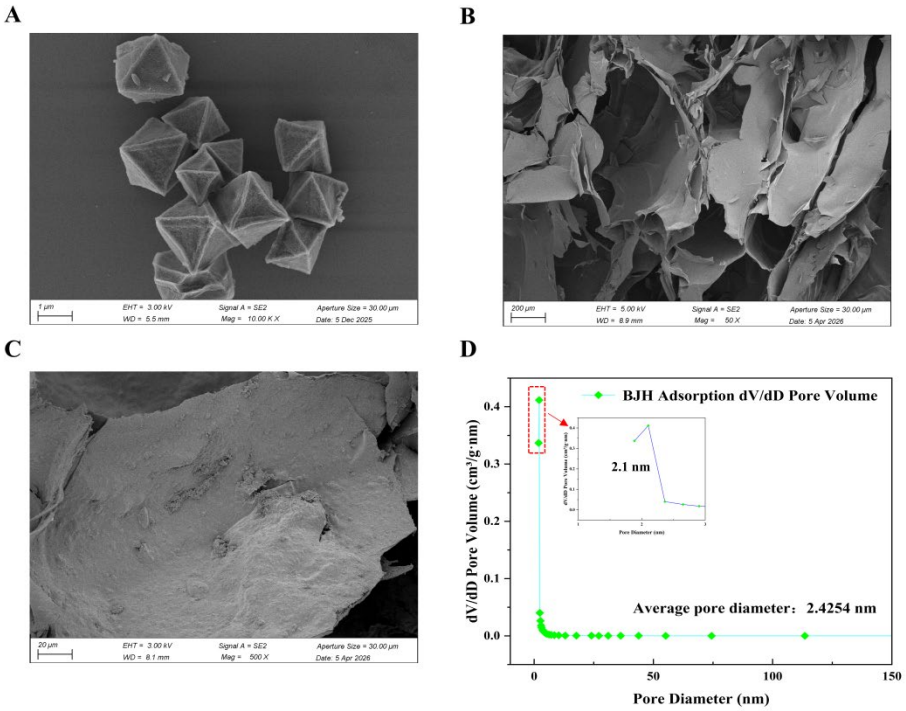

Fig. S1 Supplementary structural characterization of Fe-MOF and the Fe-MOF/SA composite. SEM images of (A) pristine Fe-MOF, (B) SA, and (C) Fe-MOF/SA. (D) BJH pore-size distribution of Fe-MOF.

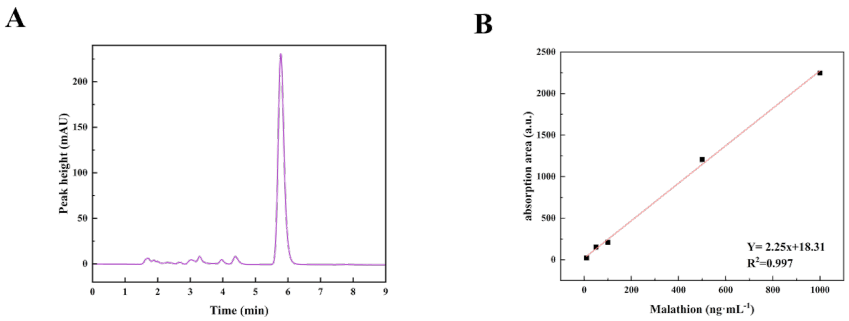

Fig. S2 HPLC chromatographic validation for malathion quantification. (A) Representative HPLC chromatogram of malathion. (B) HPLC calibration curve obtained by plotting the chromatographic peak area against malathion concentration.

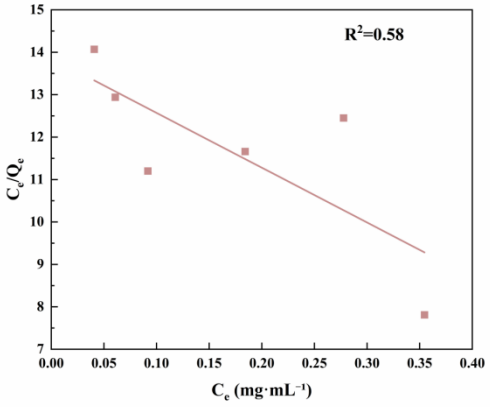

Fig. S3 Langmuir isotherm fitting of malathion adsorption on Fe-MOF.

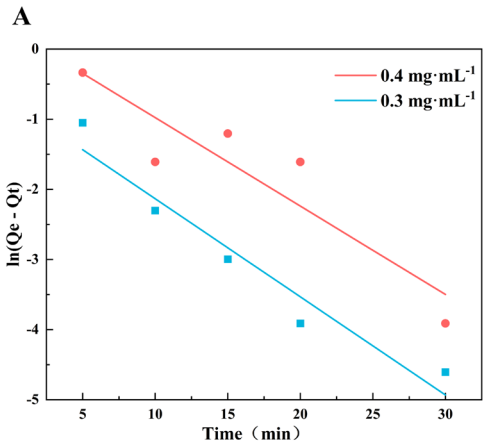

Fig. S4 Kinetic-model fitting for malathion adsorption on Fe-MOF. (A) Pseudo-first-order kinetic fitting expressed as $\ln(q_e - q_t)$ versus time.

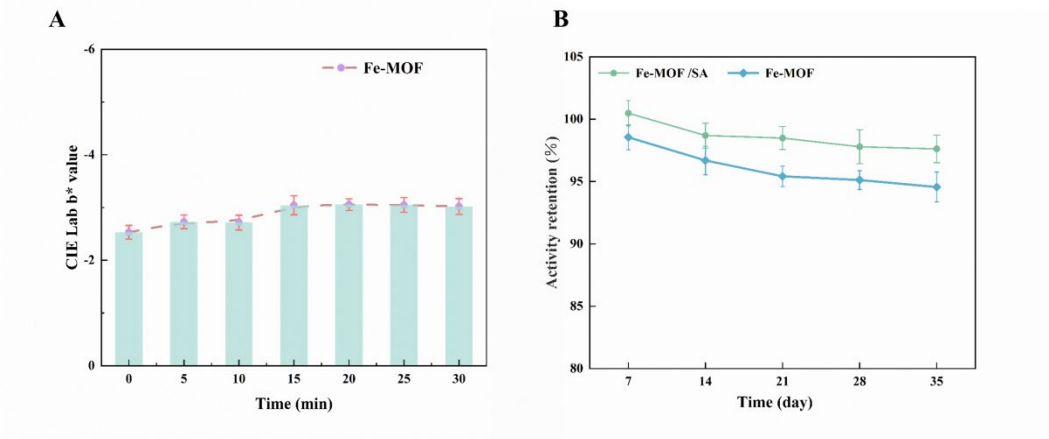

Fig. S5 (A) Time stability of the colourimetric signal after completion of the detection reaction. (B) Comparison of activity retention between free Fe-MOF and Fe-MOF/SA during storage.

Table S1 Calibration curve data points.

Malathion concentration (ng·mL^{-1})	CIE LAB b* value
10	-17.108
25	-11.137
50	-8.749
100	-2.833
250	2.084
400	3.953
500	5.033

Table S2 Limit of detection (LOD) calculation for the proposed hydrogel chip.

Parameter	Value
Calibration equation	b* = 13.03 lgC − 29.96
R^2	0.993
Blank signal replicates	10
Mean blank signal, b*blank	−21.6055
Standard deviation of blank signal, σ	0.02652

b*blank + 3σ	-21.5259
LOD	4.4

Table S3 Matrix-dependent responses of free Fe-MOF and Fe-MOF/SA hydrogel chip in representative Chinese medicinal matrices.

Matrix	Detection system	Solvent benchmark b*	Matrix b*	n	RSD (%)
Coptis	Fe-MOF	-2.83	-1.826	3	5.00
	Fe-MOF/SA		-2.848	3	3.29
Chrysanthemum	Fe-MOF	-2.83	-2.632	3	2.84
	Fe-MOF/SA		-2.867	3	1.28
Honeysuckle	Fe-MOF	-2.83	-4.099	3	2.65
	Fe-MOF/SA		-2.813	3	2.05

Table S4 Batch-to-batch reproducibility of independently prepared Fe-MOF/SA hydrogel chips.

Independent batch	Number of chips tested	Spiked concentration ($ng \cdot mL^{-1}$)	CIE LAB b* value ± SD
Batch 1	10	100	-2.873 ± 0.17
Batch 2	10	100	-2.791 ± 0.21
Batch 3	10	100	-2.844 ± 0.19

Note: The inter-batch reproducibility was assessed from the mean responses of three independently prepared batches.

Table S5 Interference-tolerance data and calculated relative signal intensity (RSI) values of the proposed Fe-MOF/SA hydrogel chip for 100 $ng \cdot mL^{-1}$ malathion in the presence of individual potential interferents.

Coexisting species	CIE LAB b* value	RSI (%)
Malathion only	-2.833	100.0
Rutin	-2.486	87.8
Tannic acid	-2.432	85.8
Glycine	-2.886	101.9
L-cysteine	-2.502	88.3

Ammonium sulfate	-2.787	98.4
Sodium chloride	-2.734	96.5
Calcium chloride	-2.789	98.4
BSA	-2.801	98.9
Dextran (70kDa)	-2.813	99.3
Dextran (200kDa)	-2.787	98.4
Chlorpyrifos	-2.701	95.3
Diazinon	-2.821	99.6
Phosmet	-2.814	99.3

Note: The response of 100 ng·mL⁻¹ malathion was evaluated in the presence of each potential interferent individually. Unless otherwise specified, the concentrations of malathion and the coexisting species were both fixed at 100 ng·mL⁻¹.

Table S6 Kinetic parameters for malathion adsorption on Fe-MOF obtained from pseudo-first-order and pseudo-second-order models.

C_0 (mg·mL^{-1})	$q_{e,exp}$ (mg·g^{-1})	Pseudo-first-order kinetic model			Pseudo-second-order kinetic model		
		k_1 (min^{-1})	$q_{e,1}$ (mg·g^{-1})	R^2	k_2(g·mg^{-1}·min^{-1})	$q_{e,2}$ (mg·g^{-1})	R^2
0.4	47.7	0.126	1.327	0.839	0.166	47.06	0.995
0.3	22.3	0.139	0.479	0.941	0.439	22.04	0.996

Table S7 Chip-to-chip repeatability of the Fe-MOF/SA hydrogel chip.

Malathion concentration (ng mL⁻¹)	n	CIE LAB b* value ± SD	RSD (%)
25	5	-11.202 ± 0.207	1.85
100	5	-2.768 ± 0.100	3.61

Table S8 Matrix-matched calibration slopes and matrix-effect calculation for malathion

detection in representative Chinese medicinal matrices.

Matrix	Calibration range (ng mL^{-1})	Solvent slope ($S_{solvent}$)	Matrix-matched slope (S_{matrix})	R^2	ME (%)
Chrysanthemum	10–500	13.03	14.08	0.991	8.05
Honeysuckle	10–500	13.03	14.78	0.995	13.44
Coptis	10–500	13.03	15.01	0.993	15.21

Table S9 Positioning of the proposed Fe-MOF/SA hydrogel chip relative to representative malathion detection strategies.

Representative method	Typical analytical role	Typical readout / instrumentation	Representative matrix context	Main practical strength	Main trade-off	Ref.
GC–MS/MS	Confirmatory residue analysis	GC–MS/MS instrumentation	Complex food / agricultural matrices after rigorous pretreatment	Excellent sensitivity, selectivity, and regulatory compatibility	Laboratory-dependent and pretreatment-intensive	40
HPLC–MS/MS	Confirmatory quantitative analysis	HPLC–MS/MS instrumentation	Complex matrices with extraction and clean-up	Robust quantification in heterogeneous samples	Limited portability and higher operational burden	41
Electrochemical sensor	Rapid screening	Electrochemical reader / electrode-based readout	Often simple or food/agricultural matrices	Fast response and convenient screening workflow	Performance may be affected by electrode fouling and device dependence	42

Aptamer / fluorescence sensor	Selective screening	Fluorescence-based readout	Often simple solutions or food-related matrices	High selectivity and potentially very low detection limits	Usually requires external instrumentation and may suffer from background interference	43
Fe-MOF/SA hydrogel chip	Portable front-end screening	Smartphone photography + ImageJ-assisted CIE LAB b* quantification	Representative pretreated Chinese medicinal matrices	Operationally simple, matrix-tolerant, and hydrogel-stabilized image-based colourimetry	Not intended for confirmatory ultra-trace quantification	This work

Table S10 Summary of cooperative factors contributing to the hydrogel-mediated matrix tolerance of the Fe-MOF/SA chip.

Cooperative factor	Proposed role in matrix tolerance	Supporting observation
Spatial confinement of Fe-MOF in the SA hydrogel	Suppresses nanozyme aggregation and helps preserve catalytic-site accessibility.	Fe-MOF particles were immobilized within the SA hydrogel framework, and the Fe-MOF/SA format showed lower matrix-dependent response deviations than free Fe-MOF in representative herbal extracts.
Stabilized local H_2O_2–TMB chromogenic microenvironment	Mitigates perturbations from matrix-derived pH, ionic strength, and co-extracted components.	The Fe-MOF/SA chip produced b*-based responses closer to the solvent benchmark in coptis, chrysanthemum, and honeysuckle extracts.
Size-selective and partitioning effect of the crosslinked SA network	Partially restricts or partitions high-molecular-weight matrix constituents, including polysaccharides and protein–polyphenol complexes.	The response deviations decreased from 35.45%, 7.00%, and 44.84% for free Fe-MOF to 0.65%, 1.31%, and 0.60% for Fe-MOF/SA in coptis, chrysanthemum, and honeysuckle extracts, respectively.

Table S11 Long-term sealed-storage stability of Fe-MOF/SA hydrogel chips under typical laboratory ambient humidity.

Storage time	Storage condition	Ambient humidity record	Test condition after storage	CIE LAB b* value	Relative response retention (%)	n
Day 0	Freshly prepared chip	Typical laboratory ambient humidity, 40–50% RH	100 ng mL^{-1} malathion under optimized conditions	-2.833	100.0	3
Day 65	Sealed storage at room temperature			-2.663 ± 0.03	94.0 ± 1.1	3